

Henry's Law Constants and Vapor–Liquid Distribution Coefficients of Noncondensable Gases Dissolved in Carbon Dioxide

Sergey B. Martynov,* Richard T.J. Porter, and Haroun Mahgerefteh

Cite This: *ACS Omega* 2022, 7, 8777–8788

Read Online

ACCESS |



Metrics & More

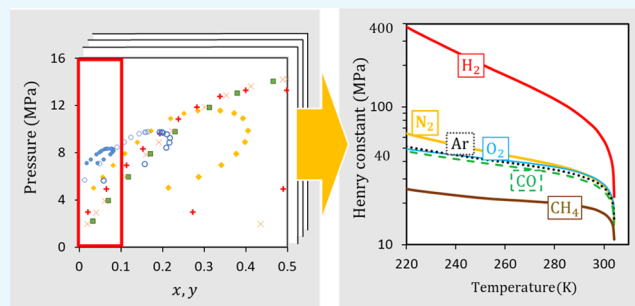


Article Recommendations



Supporting Information

ABSTRACT: The accurate determination of the solubilities of the typical impurity gases present in captured CO₂ in the carbon capture, utilization, and storage chain is an essential prerequisite for the successful modeling of the CO₂ stream thermodynamic properties. In this paper, Henry's law constants and the vapor–liquid distribution coefficients of six noncondensable gases, namely, N₂, O₂, H₂, CH₄, Ar, and CO, at infinite dilution in liquid CO₂ are derived based on published vapor–liquid equilibrium data at temperatures ranging from the triple point (216.59 K) to the critical point (304.13 K) of CO₂. The temperature dependence of Henry's law constants of the six gases is correlated using approximating functions previously proposed for aqueous solutions. A correlation that provides the best fit for the Henry constants data for all the six gases, with the accuracy (absolute average deviation %) of 4.2%, is recommended. For N₂, O₂, H₂, Ar, and CO, the combined standard uncertainty in the derived Henry constants is less than 6%, whereas for CH₄, due to a larger deviation between the utilized data, the uncertainty is less than 18%. Analysis of the temperature variation of the vapor–liquid distribution coefficient at infinite dilution shows that when all the six gases are present in the CO₂ stream, separation of N₂, O₂, Ar, and CO from CO₂ can be problematic due to their similar volatilities, while the distinct volatilities of H₂ and CH₄ at lower temperatures make their separation from CO₂ easier.



1. INTRODUCTION

Carbon capture, utilization, and storage (CCUS) refers to a collection of technologies proposed for reducing the CO₂ emissions into the atmosphere from industrial installations and combustion-based power plants. Implementation of CCUS is recognized as an essential step in decarbonizing energy-intensive industries during the transition to renewable and other alternative energy sources. One of the key factors for the successful design of CCUS using process simulation tools is the availability of accurate thermodynamic property models for CO₂ and its mixtures with other flue gas components. In particular, accurate modeling of the vapor–liquid phase equilibria (VLE) is critical for the appropriate design of the CO₂ capture, purification, and compression processes^{1–3} as well as simulation of the flow behavior in the CO₂ transportation and storage parts of the CCUS chain.⁴ Although models based on equations of state (EoSs) provide a reliable basis for predicting VLE data, their application, due to the complexity of the pertinent models and algorithms, can be difficult for use in engineering practice, for example, during the preliminary design of CO₂ capture and purification processes or flow assurance calculations for pipeline transportation networks collecting CO₂ streams of different purities from various industrial sources. In such cases, the calculation of phase equilibria in dilute solutions carrying small amounts of noncondensable gases, with dissolved gas mole fractions less than ca. 10%,⁵ can be performed with reasonable

accuracy based on Henry's law, as indeed widely used for the calculation of solubility of various components in aqueous solutions, for which extensive databases of Henry constants are readily available.⁶ However, with the exception of oxygen,^{7,8} xenon,⁹ and ozone,¹⁰ application of the above method to CO₂ is hampered by the absence of experimental data on Henry's law constants for the typical mixture components encountered in CCUS technologies.^{11,12} Obtaining the relevant experimental data is also important for validating theoretical estimates of the Henry constants, for example, those predicted based on the EoS or molecular dynamics models.^{11,13}

The aim of the present study is to address the above knowledge gap by deriving Henry's law constants from the VLE measurements for the typical to CCUS noncondensable gases mixed with CO₂. At the infinite dilution limit, the Henry constants can be obtained from the slope of the bubble line in the Px diagrams¹⁴ or with the aid of the Pxy data—using the vapor–liquid ratios y/x extrapolated to the zero dilution limit.¹⁵

Received: December 13, 2021

Accepted: February 4, 2022

Published: March 2, 2022



The latter approach is applied in the present study to determine Henry's law constants for noncondensable gases, namely, nitrogen (N₂), oxygen (O₂), hydrogen (H₂), methane (CH₄), argon (Ar), and carbon monoxide (CO), which are typically found in CO₂ streams captured from industrial installations, fossil fuel power plants, and oil refineries.¹⁶

Although the VLE data for binary mixtures of CO₂ with the above-mentioned gases have been extensively studied, particularly for N₂ and CH₄, some of the reported data are inconsistent with each other¹⁷ and scant for CO₂ mixtures with O₂, Ar, H₂, and CO.^{18–20} For binary mixtures of CO₂ with NO and C₂H₄, the phase equilibria have not yet been experimentally characterized, although attempts have been made to predict the relevant VLE data using molecular dynamics.²¹

To obtain accurate and complete P_{xy} data covering a wide range of vapor and liquid mole fractions, several studies were performed in the past 15 years, resulting in the new measurements for CO₂ binary mixtures with H₂,²² N₂,²³ Ar,²⁴ CH₄,^{25,26} O₂,²⁷ and CO.^{28–30} In the present work, the results of these studies, particularly reporting the data on noncondensable components at small dilutions (below ca. 10% mol/mol), formed the basis for determining Henry's law constants for gases dissolved in CO₂.

In practice, the application of Henry's law to binary solutions requires knowledge of the variation of the Henry constant with temperature and pressure. In particular, to describe Henry's constant dependence on temperature at the solvent saturation pressure, two approaches are commonly applied.³¹ One of these is based on the integral form of van't Hoff's equation built around a specific temperature. Constructing this approximation requires knowledge of either the enthalpy of solution or the Henry constants at two points in the relevant temperature range. Alternatively, Henry's constant variation over a wide range of temperatures is predicted using empirical correlations. For nonpolar gases, relatively simple three-parameter semi-empirical approximations have been proposed to predict the Henry constant temperature dependence at the solvent saturation conditions, up to the solvent critical temperature.^{13,32} The effect of pressure on Henry's law constants can be described using the Poynting correction, for example, in the form of the Krichevsky–Kasarnovsky equation.³³ The above may become practically important when predicting the VLE at finite dilution. In the present study, approximations are constructed for the Henry constants over a wide range of temperatures to provide the basis for VLE calculations for noncondensable gases dissolved in CO₂.

The rest of the paper is organized in three sections. Section 2 describes the method for obtaining Henry's law constants and introduces correlations describing their variation with temperature. In Section 3, the relevant VLE data for binary mixtures of the six gases with CO₂ are described and applied to obtain Henry's law constants and the vapor–liquid distribution coefficient in the infinite dilution limit. For each solute, several correlations describing the temperature variation of Henry's law constants are tested. Also, the uncertainties of newly obtained data and the accuracy of the proposed correlations are assessed. Section 4 presents the conclusions.

2. METHODOLOGY

2.1. Deriving Henry's Law Constants from VLE Data.

The solubility of a nonelectrolyte gas in a liquid in the limit of infinite dilution can be described by Henry's law⁵

$$H = \lim_{x \rightarrow 0} \frac{f^L}{x} \quad (1)$$

where f^L and x are, respectively, the fugacity and the mole fraction of the solute in the liquid phase and H is the solute's Henry's law volatility constant, hereafter referred to as the Henry constant.

For a specific pair of solute and solvent, the Henry constant variation with pressure and temperature is described by the thermodynamic relations³⁴

$$\left(\frac{\partial \ln[H/p]}{\partial p} \right)_T = - \frac{\tilde{H}^{L\infty} - \tilde{H}^{ig}}{RT^2} \quad (2)$$

$$\left(\frac{\partial \ln[H/p]}{\partial T} \right)_p = - \frac{V_i^{L\infty} - V_i^{ig}}{RT} \quad (3)$$

where $\tilde{H}^{L\infty} - \tilde{H}^{ig}$ is the heat of dissolution, represented by the difference of the partial molar enthalpies of a solute at infinite dilution and in the ideal gas state, $V_i^{L\infty}$ is the partial molar volume of a solute at the infinite dilution (where the subscript ∞ indicates the infinite dilution state), $V_i^{ig} = RT/p$ is the partial molar volume of a solute in the ideal gas state, and R is the universal gas constant.

Using a suitable enthalpy of solution and partial molar volume data, the above equations can be integrated to fully characterize H as a function of pressure and temperature. In particular, knowing H at a reference pressure and specific temperature, integral forms of eq 3, for example, the Krichevsky–Kasarnovsky equation,³³ can be used to obtain H values at elevated pressures.³⁴ Integration of eq 2 can be performed to obtain the Henry constant variation with the temperature, for example, in the form of van't Hoff's law. However, since measurements of the heat of dissolution are usually not available, eq 2 is more frequently utilized for the opposite purpose, that is, characterizing the thermal effect of dissolution based on the Henry constant data. Such data are usually derived from P_{xy} measurements at various temperatures at infinite dilution, as described next.

At finite dilution, the liquid fugacity can be defined as⁵

$$f^L = Hx\gamma^H \exp \left[\int_{p_{\text{sat}}}^p \frac{V^L(T, p, x)}{RT} dp \right] \quad (4)$$

where γ^H is the solute's activity coefficient compatible with Henry's law, V^L is the partial molar volume of the solute in the liquid phase, and p_{sat} is the saturation pressure of the pure solvent at a given temperature T .

Substituting eq 4 along with the definition of the vapor fugacity $f^V = \phi^V y p$ into the fugacity balance equation $f^V = f^L$ gives⁵

$$\phi^V y p = Hx\gamma^H \exp \left[\int_{p_{\text{sat}}}^p \frac{V^L(T, p, x)}{RT} dp \right] \quad (5)$$

where ϕ^V and y are, respectively, the solute fugacity coefficient and the mole fraction in the vapor phase. In the infinite dilution limit, $x \rightarrow 0$, eq 5 reduces to

$$H = \lim_{x \rightarrow 0} \frac{\phi^V y p}{x} \quad (6)$$

Based on this equation, with the aid of the Pxy data, H can be obtained by extrapolating isotherms $\frac{\phi^y p}{x}$ plotted as a function of x in the limit $x \rightarrow 0$, as described by Wilhelm and Battino.¹⁵ This approach is adopted in the present study.

It can be noted that the ratio of the mole fractions in eq 6 is known as the distribution coefficient (also sometimes referred to as the partition coefficient, the absolute volatility, or K -value), $K = y/x$, which plays an important role in the VLE calculations for determining the composition and the bubble and dew points of a mixture and estimating the relative volatility of the components as a measure of their potential for separation in a distillation process. Noting that at infinite dilution the total pressure approaches the saturation pressure of pure solvent, p_{sat} , H in eq 6 can be related to the distribution coefficient at infinite dilution, K^∞

$$K^\infty \equiv \lim_{x_i \rightarrow 0} K = \frac{H}{\phi^{\text{V}\infty} p_{\text{sat}}} \quad (7)$$

where $\phi^{\text{V}\infty}$ is the fugacity coefficient of the solute vapor phase at infinite dilution.

For each pair of solvent and solute, as in the case of the Henry constant, the infinite dilution distribution parameter K^∞ can be approximated as a function of temperature. Remarkably, however, near the solvent critical point, K^∞ correlates well with the solvent density^{35,36}

$$\ln(K^\infty) = 2A_{\text{Kr}} \frac{\rho_1 - \rho_{\text{cr}}}{\rho_{\text{cr}}^2 \frac{R}{M} T} \quad (8)$$

where A_{Kr} is the Krichevskii parameter that has units of pressure, ρ_1 and ρ_{cr} are, respectively, the saturated and critical densities of the solvent, and M is the molar mass of the solvent. Equation 8 shows implicitly the variation of K^∞ , and hence $H = K^\infty \phi^{\text{V}\infty} p_{\text{sat}}$, with the temperature.

2.2. Temperature Dependence of the Henry Constant.

Where the heat of dissolution remains approximately constant with temperature, the van't Hoff eq 2 can be integrated to predict the Henry constant as a function of temperature. In practice, however, the heat of dissolution varies with temperature, and therefore, constructing such an approximation becomes useful only for capturing Henry's constant variation around a specific temperature. To describe more accurately the Henry's constant behavior over a wide range of temperatures, semi-empirical correlations have been proposed for non-electrolyte solutes in water and other solvents.^{34,35}

In particular, Krause and Benson³⁷ have suggested the three-parameter correlation for the Henry constant variation with temperature

$$\ln(H) = A + B \frac{(1 - T_r)^{1/3}}{T_r^2} + C \frac{(1 - T_r)^{2/3}}{T_r^2} \quad (9)$$

where A , B , and C are the model parameters and $T_r = T/T_{\text{cr}}$ is the reduced temperature based on the critical temperature of the solvent, T_{cr} . At the solvent's critical temperature, where the Henry constant takes the value $H_{\text{cr}} \equiv H(T_{\text{cr}})$, eq 9 reduces to $\ln(H_{\text{cr}}) = A$, so that the constant A is determined by H_{cr} . The latter can be calculated directly from eq 7 where the distribution coefficient K^∞ turns to unity at the solvent critical point³⁸

$$H_{\text{cr}} = \phi_{\text{cr}}^{\text{V}\infty} p_{\text{cr}} \quad (10)$$

where p_{cr} and $\phi_{\text{cr}}^{\text{V}\infty}$ are, respectively, the solvent critical pressure and the corresponding vapor phase fugacity of the solute at infinite dilution.

Substituting the above expression for H_{cr} in eq 9 gives

$$A = \ln(\phi_{\text{cr}}^{\text{V}\infty} p_{\text{cr}}) \quad (11)$$

Based on the study by Krause and Benson³⁷ and the results of a theoretical analysis of solubility of non-polar gases near a solvent's critical point,^{38,39} Harvey³² has proposed approximating the Henry constant data in the following functional form

$$\ln\left(\frac{H}{p_{\text{sat}}}\right) = \frac{A'}{T_r} + B' \frac{(1 - T_r)^{0.355}}{T_r} + C' \frac{\exp(1 - T_r)}{T_r^{0.41}} \quad (12)$$

where the first two terms on the right-hand side are aimed at capturing the temperature variation of H near the solvent critical temperature, while the third term is introduced as an empirical correction at low temperatures.

Trinh et al.¹³ have modified eq 12 to ensure that the last term vanishes in the limit $T \rightarrow T_{\text{cr}}$

$$\ln\left(\frac{H}{p_{\text{sat}}}\right) = \frac{A''}{T_r} + B'' \frac{(1 - T_r)^{0.355}}{T_r} + C'' \left(\frac{1}{T_r} - 1\right)^{1.5} \quad (13)$$

Advantageously, the constant A'' in the above equation is determined by an additional constraint set by the theoretical limit for H_{cr} , defined by eq 10

$$A'' = \ln\left(\frac{H_{\text{cr}}}{p_{\text{cr}}}\right) = \ln(\phi_{\text{cr}}^{\text{V}\infty}) \quad (14)$$

3. RESULTS AND DISCUSSION

3.1. Deriving Henry Constants and Distribution Coefficients from Experimental Data.

Following the approach described in Section 2.1, the Henry constant data were derived based on the Pxy measurements in binary mixtures of N_2 , O_2 , H_2 , CH_4 , Ar , and CO with CO_2 , obtained from primary literature sources. The pertinent experimental database was compiled based on most recent and most accurate measurements at small dilutions ($x < 0.1$)⁵ and temperatures between the triple point (216.59 K) to the critical point of CO_2 (304.13 K). To ensure more complete coverage and better resolution of the temperature range, data from various sources were utilized, as, for example, in the case of the CO_2 - N_2 mixture for which we used the data from Westman et al.²³ and Fandiño et al.,²² the CO_2 - Ar mixture represented by the measurements from Løvseth et al.²⁴ and Coquelet et al.,⁴³ and the CO_2 - CO mixtures for which we combined the data from studies by Westman et al.,²⁸ Chapoy et al.,³⁰ and Souza et al.²⁹ For CH_4 , the Pxy data from recent experimental campaigns were found to be rather limited. In particular, Legoix et al.²⁵ have reported the bubble point data but did not include the dew point measurements, while the study by Peropoulou et al.²⁶ has only covered temperatures above 293 K. To expand our database for CH_4 to low temperatures, we have also included historical data identified in the recent literature reviews.^{18,19}

For each solute gas, based on the Pxy data, the distribution coefficients $K = y/x$ and the corresponding isotherms $\phi^{\text{V}\infty} K p$ were constructed and approximated using quadratic functions

$$\phi^{\text{V}\infty} K p = H + c_1 x + c_2 x^2 \quad (15)$$

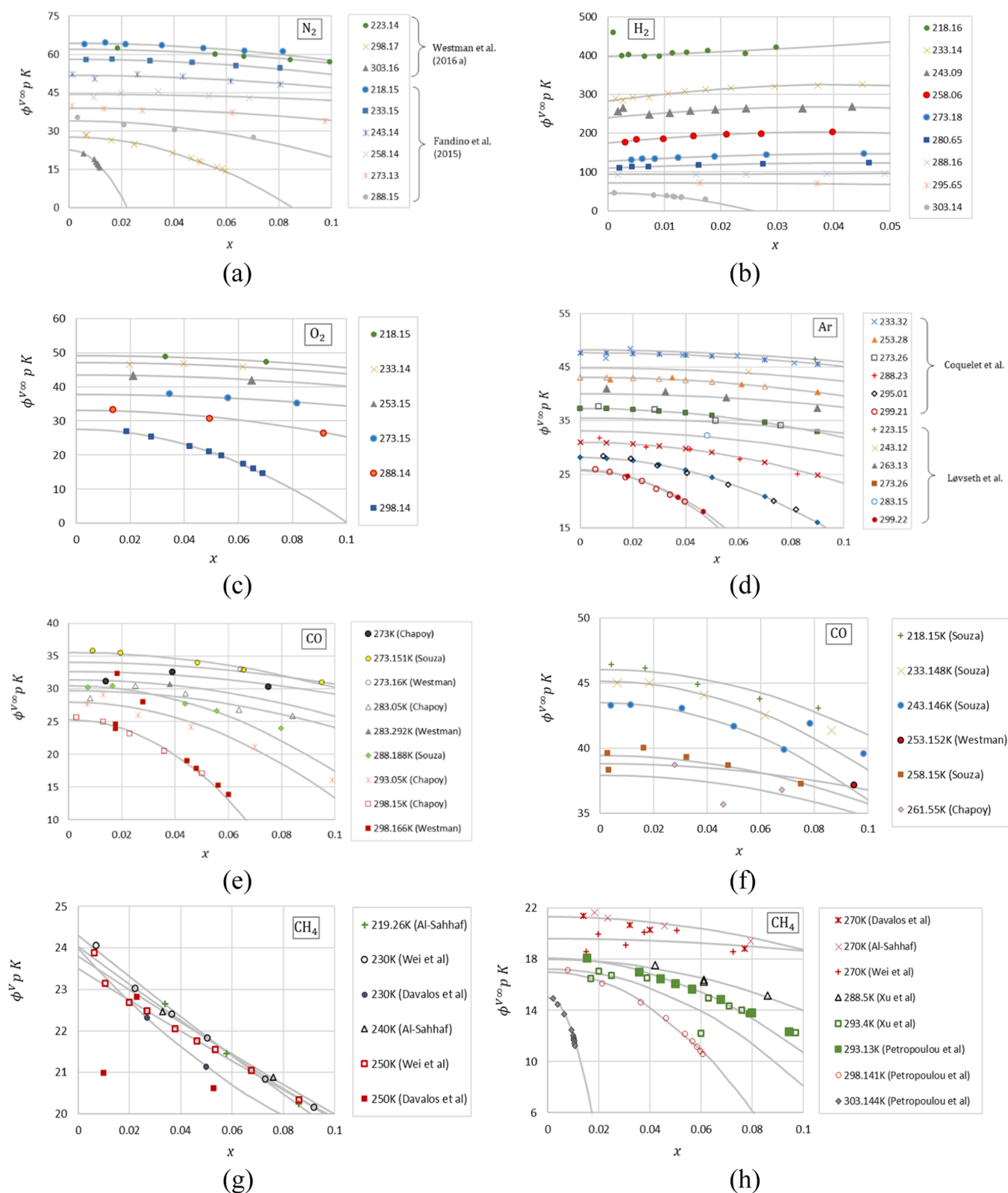


Figure 1. Variation of $K\phi_1^{\infty}p$ as a function of the liquid mole fraction at different temperatures for different gases dissolved in CO_2 . (a) N_2 , (b) H_2 , (c) O_2 , (d) Ar , (e,f) CO , and (g,h) CH_4 . Points—experimental data derived from the Pxy measurements at various temperatures (see Table 1 for references), curves—fitted quadratic approximations using eq 15.

where ϕ^{∞} were approximated by the values calculated at very small dilutions ($x = 0.0001$) using the reference EoSs in REFPROP.⁴⁰ The literature sources for the reference EoSs and the choice of mixing rules and specific parameters for each

binary mixture are detailed in the Excel file in the Supporting Information.

Figure 1 shows the $\phi^{\infty}Kp$ data plotted as a function of x and the corresponding approximations by eq 15 for various

Table 1. Values of the Henry Constants (H) and the Vapor–Liquid Distribution Coefficients at Infinite Dilution (K^∞) Derived from the Literature P_{xy} Data for the Six Gas Solutes at Various Temperatures (T) and Calculated at the Critical Point of the CO_2 Solvent Where $K_{\text{cr}}^\infty = 1$ and H_{cr} Is Obtained from eq 10^a

gas	reference	T (K)	p_{sat} (MPa)	ϕ^{V^∞} (–)	H (MPa)	$K^\infty = \frac{H}{\phi_1^{V^\infty} p_{\text{sat}}}$ (–)	
H ₂	Fandiño et al. (2015) ²²	218.16	0.55	1.093	397.50	656.18	
		233.14	1.00	1.139	282.94	247.38	
		243.09	1.43	1.180	239.81	142.65	
		258.06	2.28	1.264	175.01	60.60	
		273.18	3.49	1.400	128.46	26.32	
		280.65	4.23	1.504	109.69	17.25	
		288.16	5.09	1.658	93.38	11.07	
		295.65	6.07	1.929	72.43	6.18	
		303.14	7.21	2.792	45.41	2.26	
	theory @ T_{cr} eq 10	304.13	7.38	3.019	22.27	1	
N ₂	Westman et al. (2016) ²³	223.14	0.68	1.004	62.05	90.59	
		298.17	6.44	1.487	27.78	2.90	
		303.16	7.21	1.863	22.72	1.69	
	Fandiño et al. (2015) ²²	218.15	0.55	1.002	64.45	116.11	
		233.15	1.00	1.011	57.96	57.05	
		243.14	1.43	1.024	51.80	35.46	
		258.14	2.29	1.058	44.49	18.37	
		273.13	3.48	1.123	38.98	9.97	
		288.15	5.09	1.260	33.89	5.29	
		303.15	7.21	1.862	24.72	1.84	
theory @ T_{cr} eq 10	304.13	7.38	1.980	14.61	1		
O ₂	Westman et al. (2016) ²⁷	218.15	0.55	1.051	49.09	84.37	
		233.14	1.00	1.075	47.00	43.54	
		253.15	1.97	1.126	43.39	19.57	
		273.15	3.48	1.220	37.84	8.90	
		288.14	5.09	1.369	33.07	4.75	
		298.14	6.43	1.608	27.63	2.67	
		304.13	7.38	2.115	15.60	1	
		theory @ T_{cr} eq 10	304.13	7.38	2.115	15.60	1
		CH ₄	Petropoulou et al. (2018) ²⁶	303.14	7.21	1.411	15.04
	298.14			6.43	1.210	17.00	2.18
293.13	5.73			1.137	18.07	2.78	
Xu et al. (1992) ⁴²	288.50		5.13	1.097	18.00	3.20	
	293.40		5.76	1.139	17.22	2.62	
Davalos et al. (1976) ⁴¹	270.00		3.20	1.006	21.32	6.47	
Al-Sahhaf et al. (1993) ⁴⁴	219.26		0.58	1.009	24.30	41.57	
	240.00		1.28	1.028	23.80	18.44	

gas	reference	T (K)	p_{sat} (MPa)	ϕ^{V^∞} (–)	H (MPa)	$K^\infty = \frac{H}{\phi_1^{V^\infty} p_{\text{sat}}}$ (–)	
Ar	Wei et al. (1995) ⁴⁵	270.00	3.20	1.007	21.30	6.47	
		230.00	0.89	1.007	24.04	26.76	
		250.00	1.79	1.028	23.51	13.05	
		270.00	3.20	1.006	19.61	5.95	
		theory @ T_{cr} eq 10	304.13	7.38	1.476	10.89	1
	CO	Løvseth et al. (2018) ²⁴	223.15	0.68	1.037	48.20	68.15
			243.12	1.43	1.068	44.88	29.47
			263.13	2.65	1.125	40.06	13.45
			273.26	3.49	1.174	35.47	8.64
			283.15	4.50	1.249	33.06	5.88
Coquelet et al. (2008) ⁴³		299.22	6.59	1.569	25.67	2.48	
		233.32	1.01	1.050	47.71	44.94	
		253.28	1.98	1.092	43.10	19.96	
		273.26	3.50	1.174	37.29	9.09	
		288.23	5.10	1.307	30.96	4.65	
CO	theory @ T_{cr} eq 10	295.01	5.98	1.431	28.14	3.29	
		299.21	6.59	1.569	25.85	2.50	
		304.13	7.38	2.002	14.77	1	
		Westman et al. (2018) ²⁵	253.15	1.97	1.106	38.84	17.82
			273.16	3.49	1.173	34.09	8.34
	283.29		4.52	1.237	31.38	5.62	
	298.17		6.44	1.469	25.24	2.67	
	Chapoy et al. (2020) ³⁰		261.55	2.53	1.128	37.91	13.28
		273.00	3.47	1.172	32.67	8.03	
		283.05	4.49	1.235	29.76	5.37	
293.05		5.72	1.351	27.97	3.62		
298.15		6.43	1.468	25.34	2.68		
CO	Souza et al. (2018) ²⁹	218.15	0.55	1.056	46.05	78.74	
		233.15	1.00	1.072	45.14	41.90	
		243.15	1.43	1.087	43.52	28.04	
		258.15	2.29	1.119	39.43	15.39	
		273.15	3.49	1.173	35.57	8.70	
	theory @ T_{cr} eq 10	288.19	5.09	1.284	30.50	4.67	
		302.94	7.18	1.756	21.41	1.70	
		304.13	7.38	1.879	13.86	1	

^a p_{sat} is the saturation pressure of CO_2 , calculated using correlation by Span and Wagner provided in the Appendix.

temperatures of the six gases, fitted using the least squares method in Excel (see the Supporting Information). Analysis of the data shows that although for all the gases sufficient data are available to resolve the isotherms at $x < 0.1$, some data at low x (particularly below 0.01) are scattered, deviating significantly from the trends observed at higher x . The points that deviated significantly from the data sets have been eliminated from further analysis. These included the measurements by Fandiño et al.²² for H_2 at $x = 0.0009$, $T = 218.16$ K and $x = 0.0026$, $T = 243.09$ K (Figure 1b) and for CH_4 by Davalos et al.⁴¹ at 230 and

250 K (Figure 1g) and Xu et al.⁴² at $x = 0.0015$, $T = 288.5$ K (Figure 1h).

As can be seen from the plots in Figure 1, eq 15 adequately approximates the data. The majority of the isotherms show parabolic behavior, with the exception of almost linear trends of some of the data for H_2 (Figure 1b) and CH_4 at low temperatures (Figure 1g). There is generally good consistency in the trends for isotherms obtained from different publications. Some of the data sets obtained by different authors at the same temperatures match with each other very well [e.g., the measurements by Coquelet et al.⁴³ and Løvseth et al.²⁴ for Ar

(Figure 1d), by Souza et al.²⁹ Westman et al.,²⁸ and Chapoy et al.³⁰ for CO, except for a small number of outliers in Westman et al.'s²⁸ data at 253.152 and 298.166 K (Figure 1e,f), and by Pteropoulou et al.²⁶ and Xu et al.⁴² for CH₄ at 293 K (Figure 1h)]. The low dilution limit is particularly well resolved for H₂ (Figure 1b) and also for N₂ and Ar (Figure 1a,d, respectively). A relatively large scatter of the data can be observed in the measurements for CO (Figure 1e,f) and CH₄ (Figure 1g,h).

Table 1 presents the list of H values fitted in eq 15 and the corresponding distribution coefficients, K_{∞} , obtained for the six gases at different temperatures, along with the predicted values of the solutes' fugacity coefficients and saturation pressures of CO₂ calculated using eq 20 provided in the Appendix. The newly derived H and K_{∞} data are hereafter referred to as "experimental data". Also included in Table 1 are the theoretical estimates for H obtained at the solvent critical point using eq 10 where K^{∞} turns to unity.³⁸

3.2. Temperature Variation of the Henry Constants and the Distribution Coefficients. As can be seen in Table 1, both H and K^{∞} decrease with temperature. Given that K^{∞} and H are interrelated by eq 7, approximating the temperature variation for one of them is sufficient to determine the other. In this study, approximations for H are constructed using expressions of Section 2.2. Also, the validity of eq 8, as a basis for approximating K^{∞} and the corresponding H for a wide range of temperatures, is examined.

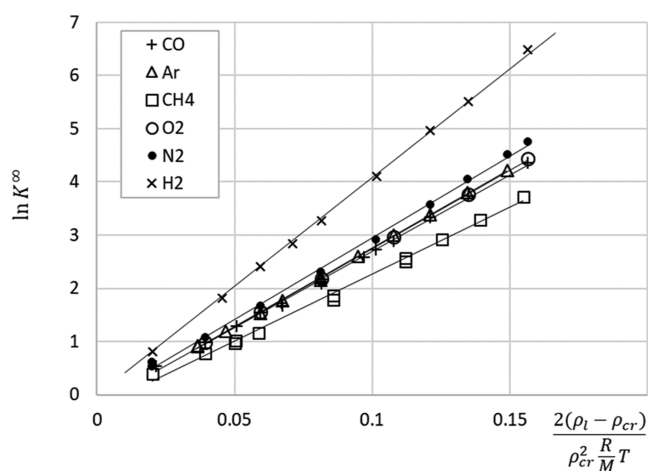


Figure 2. Variation of $\ln K^{\infty}$ as a function of the dimensionless density of the solvent at saturation for the six gases. Points—data derived from the P_{xy} measurements obtained from various sources (Table 1), lines—fitted eq 8 with the coefficients provided in Table 2.

Figure 2 shows the variation of $\ln K^{\infty}$ with $\frac{2(\rho_l - \rho_{cr})}{\rho_{cr}^2 \frac{R}{M} T}$ and the linear approximations constructed using the least squares regression of eq 8 for the six gases, performed using Excel (see the Supporting Information). The saturated liquid CO₂ density was calculated using eq 21 presented in the Appendix. The fitted values of the Krichevskii parameter are listed in Table 2. Although Figure 2 gives an impression that the linear approximations fit the data well, it must be noted that relatively small approximation errors for $\ln K^{\infty}$ can translate into relatively large uncertainties for K^{∞} and the corresponding Henry constant data, as discussed later in this section.

The observed decrease in the K^{∞} values for the gases with the temperature (see Table 2) has important practical implications in the context of separating impurities from CO₂ streams as part of the purification of captured CO₂. In particular, the data in Table 1 and Figure 2 show that

- O₂, CO, and Ar have very similar volatilities over the entire range of temperatures studied,
- the volatility of N₂ is moderately (ca. 20%) higher than that of O₂, CO, and Ar,
- the volatility of H₂ is ca. 2–9 times higher than those of O₂, CO, and Ar, and
- the volatility of CH₄ is ca. 1.5–2.5 times lower than those of O₂, CO, and Ar.

In Figure 3, the Henry constant values from Table 1, marked as "experimental data", are plotted as a function of the reduced temperature of the solvent $T_r = T/T_{cr}$, supplemented by the experimental data for O₂,^{7,8} predictions based on the molecular dynamics simulations for N₂¹² and O₂,¹¹ the theoretical estimates of H_{cr} based on eq 10, and approximations by eqs 8, 9, 12, and 13 fitted to the "experimental data" using the least squares method in MatLab (see the Supporting Information). Table 2 presents the regressed coefficients in the approximating equations, while Table 3 presents the R^2 statistics and the accuracy of the approximations expressed using the absolute average deviation (AAD).

As can be seen in Figure 3, eqs 9 and 13 both provide good approximations of the data in the entire temperature range investigated for all of the six gases. Equation 12 also approximates the data well but has the tendency of slightly underestimating the Henry constant values at T_r below ca. 0.75 ($T < 230$ K). The latter can likely be attributed to the fact that, as explained by Trinh et al.,¹³ the last term in Harvey's eq 12 is not taken in the asymptotically correct form. In the case of oxygen (Figure 3c), the Henry constant data derived from the measurements by Westman et al.²⁷ match well with the values reported by Fredenslund et al.^{7,8}

Table 2. Fitted Coefficients in eqs 8, 9, 12, and 13 Approximating the Henry Constant Variation with Temperature for Various Gases Dissolved in CO₂ (Table 1)

gas	number of data points	Harvey's correlation, eq 12			Trinh's modification of Harvey's correlation, eq 13			Krause and Benson's (1989) correlation, eq 9			Equation 8
		A'	B'	C'	A''	B''	C''	A	B	C	A_{Kr} (MPa)
N ₂	10	-18.2	1.12	19.2	0.68	3.07	4.41	2.68	120	-111	29.69
H ₂	9	-19.2	2.14	20.6	1.11	4.54	4.01	3.10	84	316	40.86
O ₂	6	-12.2	1.90	13.0	0.75	2.87	3.64	2.75	123	-132	27.75
Ar	12	-13	1.78	13.8	0.69	2.88	4.12	2.69	114	-117	27.60
CO	16	-14.6	1.50	15.4	0.63	2.91	4.03	2.63	109	-113	26.90
CH ₄	12	-16.5	0.98	17.0	0.39	2.32	4.99	2.39	71	-83	22.82

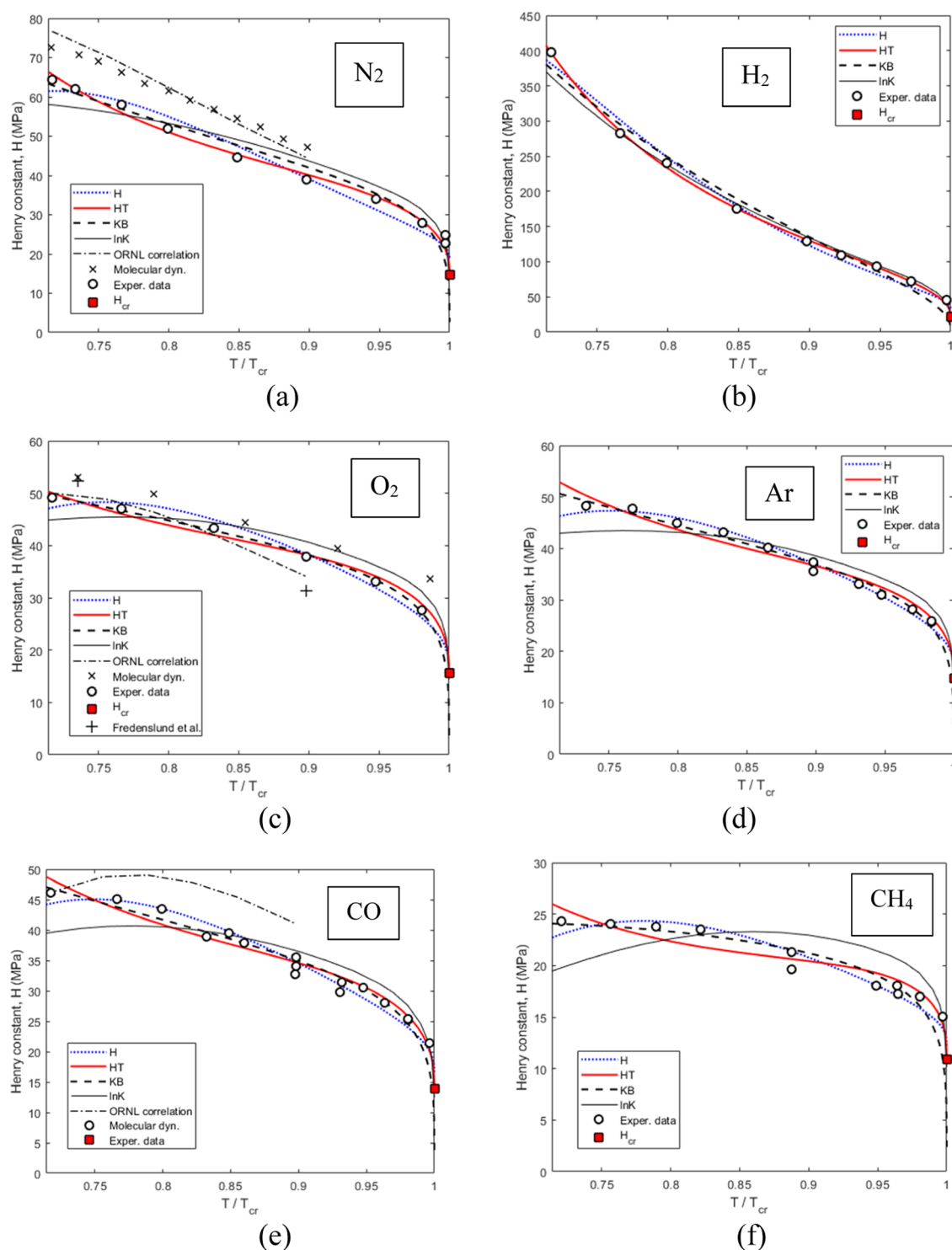


Figure 3. Henry constant variation with the temperature for various gases dissolved in CO₂. (a) N₂, (b) H₂, (c) O₂, (d) Ar, (e) CO, and (f) CH₄. Data points from Table 1 (Exper. data) are presented along with the values reported for the O₂–CO₂ system at 273.15 K⁸ and 223.75 K,⁷ the molecular dynamics simulations for the N₂–CO₂ mixture¹² and the O₂–CO₂ mixture,¹¹ and the theoretical estimates of H_{cr} based on eq 10. Curves—fitted approximations: H (dotted blue curves)—Harvey’s³² correlation, eq 12, HT (solid red curves)—Trinh et al.’s¹³ modification of Harvey’s correlation, eq 13, KB (dashed black curves)—Krause and Benson’s³⁷ correlation, eq 9, ln K (thin black curves)—eq 7 substituted in eq 8, ORNL correlation (black dashed–dotted curves) proposed by Glass and Barker⁴⁶ (see the Supporting Information).

Figure 3 also shows that correlations developed by the Oak Ridge National Laboratory (ORNL)⁴⁶ for the Henry constant at low temperatures (below 273 K) provide a reasonably good approximation of the present data for O₂ but overestimate by ca. 15% the data obtained in the present work for N₂ and CO. It also

can be seen that the molecular dynamics simulations^{11,12} tend to overestimate the Henry constants as compared to the present study, by ca. 10% for O₂ and by ca. 20% for N₂. These deviations are likely attributed to the accuracy of the experimental data used for tuning the molecular dynamics models.¹¹

Table 3. Statistics for the Constructed Approximations of the Henry Constant Variation with the Temperature (Table 2)^a

gas	number of data points	Harvey's correlation, eq 12		Trinh's modification of Harvey's correlation, eq 13		Krause and Benson's (1989) correlation, eq 9		eqs 7 and 8		
		R ²	AAD %	R ²	AAD %	R ²	AAD %	R ² (ln K)	AAD % (ln K)	AAD % (H)
N ₂	10	0.977	7.4	0.992	3.2	0.918	14.4	0.999	4.6	7.8
H ₂	9	0.992	9.9	0.999	2.3	0.983	19.1	0.9999	1.1	3.6
O ₂	6	0.986	3.6	0.992	2.3	0.803	12.7	0.999	4.1	7.2
Ar	11	0.990	2.9	0.983	3.1	0.869	8.4	0.999	4.5	7.5
CO	16	0.973	4.3	0.972	3.3	0.861	8.4	0.999	4.2	7.3
CH ₄	13	0.947	4.0	0.938	4.2	0.515	10.6	0.997	8.3	12.4

^aAAD = $\frac{1}{N} \sum_{k=1}^N \left| \frac{H_k^{\text{exp}} - H_k^{\text{fit}}}{H_k^{\text{exp}}} \right|$, where H_k^{exp} are the experimentally derived Henry constants (Table 1), H_k^{fit} are the fitted data, and N is the number of points used to build the approximation.

Returning to Table 3, the values of R^2 appear to be close to unity for all the cases, indicating the adequacy of the form of adopted approximating functions. A comparison of AADs for the different approximations shows that on average, Trinh's eq 13 gives the best fit over the entire range of temperatures (maximum AAD of 4.2%), followed by Harvey's eq 12 (maximum AAD of 7.4%), and then eq 9 proposed by Krause and Benson (with the maximum AAD of 19.1%). In the case of approximation based on eq 8, the uncertainty in approximation of $\ln K$ almost doubles when translated to the linear scale, resulting in AAD % (H) in the range from 3.6 to 12.4% for the studied six gases.

Figure 3 shows that at T_r below ca. 0.75 ($T < 230$ K), eq 8 becomes less accurate than the other correlations and hence cannot be recommended for the calculation of Henry constants at temperatures far below the critical point of the solvent.

3.3. Uncertainty Analysis. The total standard uncertainty of the Henry constant data ($u_{\text{tot}}(H)$) presented in Table 1 combines the propagated uncertainties of various quantities that determine H in eq 6, $u_{\text{exp}}(H)$, and the uncertainty of fitting H values in eq 15, $u_{\text{approx}}(H)$

$$\frac{u_{\text{tot}}(H)}{H} = \sqrt{\left(\frac{u_{\text{exp}}(H)}{H}\right)^2 + \left(\frac{u_{\text{approx}}(H)}{H}\right)^2} \quad (16)$$

The first component, $u_{\text{exp}}(H)$, is estimated based on the analysis of the error propagation in eq 6

$$\frac{u_{\text{exp}}(H)}{H} = \sqrt{\left(\frac{u(x)}{x}\right)^2 + \left(\frac{u(y)}{y}\right)^2 + \left(\frac{u(p)}{p}\right)^2 + \left(\frac{u(\phi^{\text{V}\infty})}{\phi^{\text{V}\infty}}\right)^2} \quad (17)$$

where $u(x)$, $u(y)$, and $u(p)$ are standard uncertainties of the corresponding experimentally observed quantities x , y , and p and $u(\phi^{\text{V}\infty})$ is the uncertainty of $\phi^{\text{V}\infty}$ estimated as described next.

Given that the fugacity coefficient is the quantity which is not measured directly but rather calculated based on the reference EoSs in REFPROP⁴⁰ (see the details in the EOS validation section in the Excel file provided in the Supporting Information), the uncertainty $u(\phi^{\text{V}\infty})$ carries the components associated with (a) the inaccuracy of the underlying predicting model and (b) the uncertainty propagated from the variables that the fugacity coefficient depends upon (e.g., pressure and composition). Given that the reference EoSs enable a very accurate representation of VLE data, at least at small dilutions

(see the Supporting Information), it can be assumed that the corresponding uncertainty of predictions $\phi^{\text{V}\infty}$ is negligibly small (although rigorous assessment of the accuracy of the fugacity coefficient model is beyond the scope of the present study) as compared to the experimental component of $u(\phi^{\text{V}\infty})$ due to the propagation of the errors of the pressure measurements $u(p)$

$$u(\phi^{\text{V}\infty}) = \frac{d\phi^{\text{V}\infty}}{dp_{\text{sat}}} u(p) \quad (18)$$

When using this equation, the derivative term was approximated as

$$\frac{d\phi^{\text{V}\infty}}{dp_{\text{sat}}} \approx \frac{\phi^{\text{V}\infty}(p_{\text{sat}} + u(p)) - \phi^{\text{V}\infty}(p_{\text{sat}})}{u(p)} \quad (19)$$

In eq 16, the second component of the combined total uncertainty, $u_{\text{approx}}(H)$, was obtained as the standard deviation of H fitted using the least square method in eq 15.

Table 4 presents the list of the individual components and the total combined uncertainty of H for the six gases at various temperatures. The relative uncertainty $u_{\text{approx}}(H)/H$ is generally smaller or of the same order of magnitude as the relative experimental uncertainty of the mole fraction measurements, while $u(p)/p$ and $u(\phi^{\text{V}\infty})/\phi^{\text{V}\infty}$ have the smallest contribution to $u_{\text{tot}}(H)$. For N₂, O₂, H₂, Ar, and CO, the total combined uncertainty of the derived H values, $u_{\text{tot}}(H)/H$, is less than ca. 4.7% (this applies to the majority of the data points, except for a few points near the critical temperature of CO₂, where the uncertainty goes up to 6.13%), while for CH₄, due to a larger relative uncertainty of the solute liquid fraction measurements, $u(x)/x$, the total combined uncertainty is the largest among the six gases studied (average 7%, maximum 18%).

4. CONCLUSIONS

The Henry constants and the infinite dilution vapor–liquid distribution coefficients were obtained for six noncondensable gas components, namely, N₂, H₂, O₂, Ar, CO, and CH₄, commonly present as impurities in the captured CO₂ streams in the CCUS chain. The data were determined based on the most reliable Pxy measurements covering the entire range of practically relevant temperatures spanning from the triple point of CO₂ (216.59 K) to its critical point (304.13 K) and the fugacity coefficients of the gases estimated using the reference EoSs in REFPROP.⁴⁰

The accuracy of the derived Henry constants was found to be largely dependent on the quality of the utilized experimental Pxy

Table 4. Relative Experimental Uncertainties of the Liquid and Vapor Mole Fractions [$u(y)/y$ and $u(x)/x$], the Standard Uncertainty of Fitting the Henry Constants ($u_{\text{approx}}(H)/H$) in eq 12, and the Total Standard Uncertainty of H , $u_{\text{tot}}(H)$, Estimated using eq 17^a

gas	reference	T (K)	H (MPa)	$\frac{u_{\text{approx}}(H)}{H}$ (%)	$\frac{u(y)}{y}$ (%)	$\frac{u(x)}{x}$ (%)	$\frac{u(p)}{p}$ (%)	$\frac{u(\phi^{V\infty})}{\phi^{V\infty}}$ (%)	$\frac{u_{\text{tot}}(H)}{H}$ (%)
H ₂	Fandiño et al. (2015) ²²	218.16	397.50	1.00	0.67	2.08	0.54	0.02	2.47
		233.14	282.94	0.65	0.84	3.85	0.30	0.03	4.00
		243.09	239.81	1.28	0.88	2.94	0.21	0.03	3.33
		258.06	175.01	0.81	0.94	1.67	0.13	0.03	2.08
		273.18	128.46	0.51	1.00	1.22	0.09	0.04	1.66
		280.65	109.69	0.51	1.06	2.50	0.07	0.05	2.76
		288.16	93.38	0.17	1.08	2.94	0.06	0.07	3.14
		295.65	72.43	0.28	1.01	1.08	0.05	0.11	1.51
		303.14	45.41	1.77	2.00	4.55	0.04	0.25	5.30
N ₂	Westman et al. (2016) ²³	223.138	62.05	0.59	0.05	1.46	0.03	0.00	1.58
		298.174	27.78	1.02	1.64	4.21	0.02	0.02	4.64
		303.158	22.72	1.59	3.31	4.91	0.02	0.05	6.13
	Fandiño et al. (2015) ²²	218.147	64.45	0.23	0.68	1.09	0.31	0.00	1.34
		233.151	57.96	0.20	0.82	1.09	0.21	0.01	1.39
		243.138	51.80	1.09	1.05	3.85	0.20	0.01	4.14
		258.144	44.49	1.68	0.95	1.09	0.11	0.01	2.22
		273.128	38.98	0.71	1.09	4.55	0.08	0.02	4.73
		288.152	33.89	2.79	1.08	1.56	0.06	0.04	3.38
303.153	24.72	2.68	1.09	2.00	0.04	0.13	3.53		
O ₂	Westman et al. (2016) ²⁷	218.15	49.09	0.44	0.13	1.45	0.09	0.00	1.52
		233.14	47.00	0.32	0.12	2.48	0.05	0.00	2.50
		253.15	43.39	0.18	0.18	2.28	0.03	0.00	2.30
		273.15	37.84	0.82	0.64	1.39	0.03	0.01	1.74
		288.14	33.07	1.27	0.84	3.55	0.02	0.02	3.87
		298.14	27.63	0.56	1.10	2.58	0.02	0.03	2.86
CH ₄	Petropoulou et al. (2018) ²⁶	293.13	18.07	0.74	0.35	0.65	0.02	0.01	1.05
		298.141	17.00	0.65	0.70	1.24	0.02	0.01	1.57
		303.144	15.04	0.27	3.61	4.78	0.02	0.02	6.00
	Xu et al. (1992) ⁴²	288.5	18.00	1.64	1.92	6.67	0.75	0.26	7.17
		293.4	17.22	4.28	2.50	5.88	0.81	0.42	7.74
	Davalos et al. (1976) ⁴¹	270	21.32	2.28	1.20	17.86	0.14	0.01	18.04
	Al-Sahhaf et al. (1993) ⁴⁴	219.26	24.30	0.76	0.57	5.90	0.14	0.00	5.98
		240	23.80	0.23	0.57	6.10	0.14	0.00	6.13
		270	21.30	0.93	1.91	10.93	0.14	0.01	11.13
	Wei et al. (1995) ⁴⁵	230	24.04	0.36	1.29	7.14	0.10	0.10	7.27
		250	23.51	0.20	2.56	7.69	0.10	0.10	8.11
		270	19.61	2.53	2.61	3.31	0.10	0.10	4.92
Ar	Løvseth et al. (2018) ²⁴	223.15	48.20	0.00	0.02	0.02	0.13	0.00	0.13
		243.12	44.88	1.30	0.02	0.24	0.02	0.00	1.32
		263.13	40.06	1.14	0.12	1.49	0.04	0.00	1.88
		273.26	35.47	0.00	0.04	0.12	0.02	0.00	0.13
		283.15	33.06	1.24	0.07	0.31	0.02	0.01	1.28
		299.22	25.67	0.63	0.36	0.83	0.02	0.03	1.10
	Coquelet et al. (2008) ⁴³	233.32	47.71	1.06	1.60	1.60	0.02	0.00	2.50
		253.28	43.10	0.60	1.60	1.60	0.01	0.00	2.34
		273.26	37.29	1.01	1.60	1.60	0.01	0.00	2.48
		288.23	30.96	1.38	1.60	1.60	0.01	0.00	2.65
		295.01	28.14	0.79	1.60	1.60	0.00	0.01	2.40
		299.21	25.85	0.48	1.60	1.60	0.00	0.01	2.31
CO	Westman et al. (2018) ²⁸	253.15	38.84	1.11	0.05	0.05	0.21	0.01	1.14
		273.16	34.09	1.24	0.10	0.50	0.03	0.01	1.34
		283.29	31.38	1.74	0.17	0.84	0.02	0.01	1.94
		298.17	25.24	0.74	0.66	1.81	0.02	0.02	2.07
	Chapoy et al. (2020) ³⁰	261.55	37.91	2.01	1.10	1.10	0.20	0.02	2.55
		273.00	32.67	1.37	1.10	1.10	0.20	0.04	2.08
		283.05	29.76	2.33	1.10	1.10	0.14	0.06	2.81

Table 4. continued

gas	reference	T (K)	H (MPa)	$\frac{u_{\text{approx}}(H)}{H}$	$\frac{u(y)}{y}$	$\frac{u(x)}{x}$	$\frac{u(p)}{p}$	$\frac{u(\phi^{\text{V}\infty})}{\phi^{\text{V}\infty}}$	$\frac{u_{\text{tot}}(H)}{H}$
				(%)	(%)	(%)	(%)	(%)	(%)
		293.05	27.97	2.32	1.10	1.10	0.14	0.11	2.80
		298.15	25.34	1.04	1.10	1.10	0.11	0.12	1.88
	Souza et al. (2018) ²⁹	218.15	46.05	0.68	1.10	1.10	1.62	0.04	2.35
		233.15	45.14	0.14	0.22	1.01	1.62	0.06	1.93
		243.15	43.52	0.29	0.19	0.90	1.62	0.08	1.89
		258.15	39.43	0.87	0.25	0.74	1.62	0.13	2.01
		273.15	35.57	0.59	0.42	0.54	1.62	0.31	1.88
		288.19	30.50	0.81	0.38	1.03	0.90	0.51	1.69
		302.94	21.41	1.33	0.31	0.83	0.90	1.80	5.29

^aThe relative standard uncertainties of the pressure measurements $u(p)/p$ were obtained based on the experimental uncertainties $u(p)$. The relative standard uncertainty of the fugacity coefficient $u(\phi^{\text{V}\infty})/\phi^{\text{V}\infty}$ was calculated based on eq 18. The uncertainties $u(y)/y$ and $u(x)/x$ were either taken from the experimental studies^{29,30,43} or estimated as a ratio of the reported absolute experimental uncertainties divided by the smallest measured mole fraction. The uncertainty $u(x)$ by Wei et al.⁴⁵ was estimated to be 0.0005 based on the data reported to four significant figures.

data at small dilutions. The estimated combined uncertainty of the derived Henry constants is less than ca. 6% for N₂, H₂, O₂, Ar, and CO. For CH₄, the utilized experimental data carried relatively large uncertainties of the gas solubility measurements at small dilutions, resulting in the Henry constant uncertainties being as large as 18%.

The experimentally derived data were supplemented by the theoretical estimates for Henry constants at the critical temperature of the CO₂ solvent (304.13 K). These estimates were found to be highly consistent with the experimentally derived data for all the gases studied, enabling better resolution of the temperature region near the critical point where the Henry constant attains its minimum.

Several empirical correlations, previously proposed for aqueous solutions, were tested to approximate the Henry constants' variation with temperature. These included the correlations by Harvey,³² Krause and Benson,³⁷ Trinh et al.,¹³ and the model based on the asymptotic behavior of the vapor–liquid distribution coefficient near the critical point utilizing the Krichevskii parameter. The correlation proposed by Trinh et al.,¹³ which is a modified version of Harvey's³² equation, was found to best approximate the Henry constant variation with the temperature for all the six gases, with the estimated maximum AAD of 4.2%.

Along with the Henry constants, the vapor–liquid distribution coefficients of the gases in the limit of infinite dilution in CO₂, which provide a measure of relative volatility of the solutes, were derived to aid the design of CO₂ separation, purification, and transportation processes. Among the six gases examined, H₂ has the highest volatility, followed by N₂ and CO, Ar and O₂ with very similar volatilities, and then CH₄, which has the lowest volatility over the entire range of temperatures examined. The data obtained show that volatilities of all the gases decrease with the temperature. Remarkably, based on the results, it can be concluded that when all the six gases are present in the CO₂ stream, separation of N₂, O₂, Ar, and CO from CO₂ can be problematic due to their similar volatilities, while distinct volatilities of H₂ and CH₄ at lower temperatures make their separation from CO₂ easier. This finding is important in the context of selecting the appropriate operating conditions and design of the gas stripping and purification steps for separation of noncondensable gases from the captured CO₂ stream.

It is important to note that Henry's law is a limiting law, and therefore, the Henry constants and the corresponding vapor–

liquid distribution coefficients are defined in the limit of infinite dilution at the solvent saturation conditions. Based on Henry's law, simple models can be constructed to enable the calculation of the VLE at finite dilutions. It should be noted that the accuracy of such models ultimately depends on the validity of the underlying assumptions and the closure models (predicting, e.g., the solute activity and fugacity coefficients) that need to be assessed by comparing the VLE predictions with the real data for a specific solute–solvent pair over the range of the gas solubilities of interest. Further work is needed to establish the ranges of validity of any Henry's law-based models for the calculation of the VLE in CO₂ solutions at finite dilutions.

Given the limited availability of the relevant P_{xy} data, the present study was limited to the characterization of the Henry constants only for the above listed six gases. For other noncondensable gases typically present in CO₂ mixtures encountered in CCUS, such as, for example, NO and C₂H₄, the P_{xy} data are not available over a wide range of temperatures and need to be obtained, either experimentally or using verified molecular dynamics models,^{11,21} as a basis for the derivation of the Henry constants.

APPENDIX

To calculate the saturation pressure of CO₂, the equation proposed by Span and Wagner⁴⁷ was applied

$$\ln\left(\frac{p_{\text{sat}}}{p_{\text{cr}}}\right) = \frac{T_{\text{cr}}}{T} \cdot \left[\sum_{i=1}^4 a_i \left(1 - \frac{T}{T_{\text{cr}}}\right)^{n_i} \right] \quad (20)$$

where $T_{\text{cr}} = 304.1282$ K and $p_{\text{cr}} = 7.3773$ MPa are the critical point temperature and pressure of pure CO₂, while a_i and n_i are constants: $a = -7.0602087$, $a_2 = 1.9391218$, $a_3 = -1.6463597$, $a_4 = -3.2995634$, $n_1 = 1$, $n_2 = 1.5$, $n_3 = 2$, $n_4 = 4$. This equation is valid in the range of temperatures from the triple point of CO₂ ($T_{\text{tr}} = 216.592$ K) to the critical point, describing the saturation pressure with the relative uncertainty of 0.012%.

The density of saturated liquid CO₂ was calculated as⁴⁷

$$\ln\left(\frac{\rho_1}{\rho_{\text{cr}}}\right) = \sum_{i=1}^4 b_i \left(1 - \frac{T}{T_{\text{cr}}}\right)^{m_i} \quad (21)$$

where $\rho_{\text{cr}} = 467.6$ kg/m³ is the critical density of pure CO₂, while a_i and n_i are constants: $b_1 = 1.9245108$, $b_2 = -0.6238555$, $b_3 = -0.32731127$, $b_4 = 0.39245142$, $m_1 = 0.34$, $m_2 = 1/2$, $m_3 = 10/6$,

$m_4 = 11/6$. This equation is valid in the range of temperatures from the triple point of CO₂ to the critical point, describing the saturated density with the relative uncertainties of 0.015, 0.04, and 1% for temperatures below 295, 303 K, and the critical point, respectively.

■ ASSOCIATED CONTENT

SI Supporting Information

The Supporting Information is available free of charge at <https://pubs.acs.org/doi/10.1021/acsomega.1c07044>.

Original and processed data (Martynov–Henry constants—supporting_information.xlsx) (XLS)

MatLab script for fitting the Henry constants as a function of temperature and plotting Figure 3 (Martynov–Henry constants—matlab_script.m) (TXT)

■ AUTHOR INFORMATION

Corresponding Author

Sergey B. Martynov – Department of Chemical Engineering, University College London, London WC1E 7JE, U.K.;
orcid.org/0000-0002-6596-1158; Email: s.martynov@ucl.ac.uk

Authors

Richard T.J. Porter – Department of Chemical Engineering, University College London, London WC1E 7JE, U.K.;
orcid.org/0000-0003-1607-1922

Haroun Mahgerefteh – Department of Chemical Engineering, University College London, London WC1E 7JE, U.K.;
orcid.org/0000-0003-3768-1885

Complete contact information is available at:
<https://pubs.acs.org/doi/10.1021/acsomega.1c07044>

Notes

The authors declare no competing financial interest.

■ ACKNOWLEDGMENTS

The lead author (S.B.M.) is grateful to Professors Lars Jørgen Christiansen, Jadran Vrabec and Solomon Brown, and Dr. Livio Ruffine for sharing additional background information and useful discussions. This work has received funding from the European Union's Horizon 2020 research and innovation program under grant agreement no. 884418. The work reflects only the authors' views and the European Union is not liable for any use that may be made of the information contained therein.

■ REFERENCES

- (1) Porter, R. T. J.; Fairweather, M.; Kolster, C.; Mac Dowell, N.; Shah, N.; Woolley, R. M. Cost and Performance of Some Carbon Capture Technology Options for Producing Different Quality CO₂ Product Streams. *Int. J. Greenh. Gas Control* **2017**, *57*, 185–195.
- (2) Martynov, S. B.; Daud, N. K.; Mahgerefteh, H.; Brown, S.; Porter, R. T. J. Impact of Stream Impurities on Compressor Power Requirements for CO₂ Pipeline Transportation. *Int. J. Greenh. Gas Control* **2016**, *54*, 652–661.
- (3) Porter, R.; Barnett, J.; Cobden, P.; de Coninck, E.; Mahgerefteh, H.; Manzolini, G.; Martynov, S.; Ruggier, F.; Spallina, V. Challenges and Opportunities of Achieving European CO₂ Transportation and Storage Specifications for Carbon Capture in the Iron and Steel Industry. *TCCS-11-Trondheim Conference on CO₂ Capture, Transport and Storage Trondheim, Norway-June 21–23, 2021*: Trondheim, Norway, 2021; pp 1–8.
- (4) Porter, R. T. J.; Mahgerefteh, H.; Brown, S.; Martynov, S.; Collard, A.; Woolley, R. M.; Fairweather, M.; Falle, S. A. E. G.; Wareing, C. J.; Nikolaidis, I. K.; Boulougouris, G. C.; Peristeras, L. D.; Tsangaris, D. M.; Economou, I. G.; Salvador, C.; Zanganeh, K.; Wigston, A.; Najafali, J. N.; Shafeen, A.; Beigzadeh, A.; Farret, R.; Gombert, P.; Hebrard, J.; Proust, C.; Ceroni, A.; Flauw, Y.; Zhang, Y.; Chen, S.; Yu, J.; Talemi, R. H.; Bensabat, J.; Wolf, J. L.; Rebscher, D.; Niemi, A.; Jung, B.; Dowell, N. M.; Shah, N.; Kolster, C.; Mechleri, E.; Krevor, S. Techno-economic assessment of CO₂ quality effect on its storage and transport: CO₂QUEST. *Int. J. Greenh. Gas Control* **2016**, *54*, 662–681.
- (5) Reid, R. C.; Prausnitz, J. M.; Poling, B. E. *The Properties of Gases and Liquids*, 5th ed.; McGraw-Hill: NY, USA, 2001.
- (6) Sander, R. Compilation of Henry's Law Constants (Version 4.0) for Water as Solvent. *Atmos. Chem. Phys.* **2015**, *15*, 4399–4981.
- (7) Fredenslund, A.; Mollerup, J.; Persson, O. Gas-Liquid Equilibrium of Oxygen-Carbon Dioxide System. *J. Chem. Eng. Data* **1972**, *17*, 440–443.
- (8) Fredenslund, A.; Sather, G. A. Gas-Liquid Equilibrium of the Oxygen-Carbon Dioxide System. *J. Chem. Eng. Data* **1970**, *15*, 17–22.
- (9) Ackley, R. D.; Notz, K. J. *The Distribution of Xenon Between Gaseous and Liquid CO₂*, 1976. ORNL-5122.
- (10) Lundin, M. D.; Danby, A. M.; Akien, G. R.; Binder, T. P.; Busch, D. H.; Subramaniam, B. Liquid CO₂ as a Safe and Benign Solvent for the Ozonolysis of Fatty Acid Methyl Esters. *ACS Sustain. Chem. Eng.* **2015**, *3*, 3307–3314.
- (11) Huang, Y.-L.; Miroshnichenko, S.; Hasse, H.; Vrabec, J. Henry's Law Constant from Molecular Simulation: A Systematic Study of 95 Systems. *Int. J. Thermophys.* **2009**, *30*, 1791–1810.
- (12) Vrabec, J.; Kedia, G. K.; Buchhauser, U.; Meyer-Pittroff, R.; Hasse, H. Thermodynamic Models for Vapor-Liquid Equilibria of Nitrogen + Oxygen + Carbon Dioxide at Low Temperatures. *Cryogenics* **2009**, *49*, 72–79.
- (13) Trinh, T.-K.-H.; De Hemptinne, J.-C.; Lugo, R.; Ferrando, N.; Passarello, J.-P. Hydrogen Solubility in Hydrocarbon and Oxygenated Organic Compounds. *J. Chem. Eng. Data* **2016**, *61*, 19–34.
- (14) de Hemptinne, J.-C.; Ledanois, J.-M.; Mougin, P.; Barreau, A. *Select Thermodynamic Models for Process Simulation-A Practical Guide Using a Three Steps Methodology*; Editions Technip, 2012.
- (15) Wilhelm, E.; Battino, R. Partial Molar Volumes of Gases Dissolved in Liquids. *Volume Properties: Liquids, Solutions and Vapours*; The Royal Society of Chemistry, 2015; pp 273–306.
- (16) Porter, R. T. J.; Fairweather, M.; Pourkashanian, M.; Woolley, R. M. The Range and Level of Impurities in CO₂ Streams from Different Carbon Capture Sources. *Int. J. Greenh. Gas Control* **2015**, *36*, 161–174.
- (17) Li, H.; Wilhelmsen, Ø.; Yan, J. Properties of CO₂ Mixtures and Impacts on Carbon Capture and Storage. *Handbook of Clean Energy Systems*; John Wiley & Sons, 2014; Vol. 1–17.
- (18) Munkejord, S. T.; Hammer, M.; Løvseth, S. W. CO₂ Transport: Data and Models - A Review. *Appl. Energy* **2016**, *169*, 499–523.
- (19) Li, H.; Jakobsen, J. P.; Wilhelmsen, Ø.; Yan, J. PVTxy Properties of CO₂ Mixtures Relevant for CO₂ Capture, Transport and Storage: Review of Available Experimental Data and Theoretical Models. *Appl. Energy* **2011**, *88*, 3567–3579.
- (20) Kroenlein, K.; Diky, V.; Muzny, C. D.; Chirico, R. D.; Magee, J. W.; Frenkel, M. ThermoLit-NIST Literature Report Builder for Thermophysical and Thermochemical Property Measurements. *NIST Standard Reference Database #171*, 2016. NIST, Applied Chemicals and Materials Division.
- (21) Lachet, V.; Creton, B.; De Bruin, T.; Bourasseau, E.; Desbiens, N.; Wilhelmsen, Ø.; Hammer, M. Equilibrium and Transport Properties of CO₂+N₂O and CO₂+NO Mixtures: Molecular Simulation and Equation of State Modelling Study. *Fluid Phase Equilib.* **2012**, *322*–323, 66–78.
- (22) Fandiño, O.; Trusler, J. P. M. M.; Vega-Maza, D. Phase Behavior of (CO₂+H₂) and (CO₂+N₂) at Temperatures between (218.15 and 303.15)K at Pressures up to 15MPa. *Int. J. Greenh. Gas Control* **2015**, *36*, 78–92.
- (23) Westman, S. F.; Stang, H. G. J.; Løvseth, S. W.; Austegard, A.; Snustad, I.; Storset, S. Ø.; Ertesvåg, I. S. Vapor-Liquid Equilibrium Data

for the Carbon Dioxide and Nitrogen ($\text{CO}_2 + \text{N}_2$) System at the Temperatures 223, 270, 298 and 303 K and Pressures up to 18 MPa. *Fluid Phase Equilib.* **2016**, *409*, 207–241.

(24) Løvseth, S. W.; Austegard, A.; Westman, S. F.; Stang, H. G. J.; Herrig, S.; Neumann, T.; Span, R. Thermodynamics of the Carbon Dioxide plus Argon ($\text{CO}_2 + \text{Ar}$) System: An Improved Reference Mixture Model and Measurements of Vapor-Liquid, Vapor-Solid, Liquid-Solid and Vapor-Liquid-Solid Phase Equilibrium Data at the Temperatures 213–299 K and Pressures Up. *Fluid Phase Equilib.* **2018**, *466*, 48–78.

(25) Legoix, L.; Ruffine, L.; Donval, J. P.; Haeckel, M. Phase Equilibria of the $\text{CH}_4\text{-CO}_2$ Binary and the $\text{CH}_4\text{-CO}_2\text{-H}_2\text{O}$ Ternary Mixtures in the Presence of a CO_2 -Rich Liquid Phase. *Energies* **2017**, *10*, 2034.

(26) Petropoulou, E.; Voutsas, E.; Westman, S. F.; Austegard, A.; Stang, H. G. J.; Løvseth, S. W. Vapor-Liquid Equilibrium of the Carbon Dioxide/Methane Mixture at Three Isotherms. *Fluid Phase Equilib.* **2018**, *462*, 44–58.

(27) Westman, S. F.; Stang, H. G. J.; Løvseth, S. W.; Austegard, A.; Snustad, I.; Ertesvåg, I. S. Vapor-Liquid Equilibrium Data for the Carbon Dioxide and Oxygen ($\text{CO}_2 + \text{O}_2$) System at the Temperatures 218, 233, 253, 273, 288 and 298 K and Pressures up to 14 MPa. *Fluid Phase Equilib.* **2016**, *421*, 67–87.

(28) Westman, S. F.; Austegard, A.; Stang, H. G. J.; Løvseth, S. W. Vapor-Liquid Equilibrium Data for the Carbon Dioxide and Carbon Monoxide ($\text{CO}_2 + \text{CO}$) System at the Temperatures 253, 273, 283 and 298 K and Pressures up to 13 MPa. *Fluid Phase Equilib.* **2018**, *473*, 37–49.

(29) Souza, L. F. S.; Al Ghafri, S. Z. S.; Trusler, J. P. M. Measurement and Modelling of the Vapor-Liquid Equilibrium of ($\text{CO}_2 + \text{CO}$) at Temperatures between (218.15 and 302.93) K at Pressures up to 15 MPa. *J. Chem. Thermodyn.* **2018**, *126*, 63–73.

(30) Chapoy, A.; Ahmadi, P.; de Oliveira Cavalcanti Filho, V.; Jadhwar, P. Vapor-Liquid Equilibrium Data for the Carbon Dioxide (CO_2) + Carbon Monoxide (CO) System. *J. Chem. Thermodyn.* **2020**, *150*, 106180.

(31) Smith, F. L.; Harvey, A. H. Avoid Common Pitfalls When Using Henry's Law. *Chem. Eng. Prog.* **2007**, *103*, 33–39.

(32) Harvey, A. H. Semiempirical Correlation for Henry's Constants over Large Temperature Ranges. *AIChE J.* **1996**, *42*, 1491–1494.

(33) Krichevsky, I. R.; Kasarnovsky, J. S. Thermodynamical Calculations of Solubilities of Nitrogen and Hydrogen in Water at High Pressures. *J. Am. Chem. Soc.* **1935**, *57*, 2168–2171.

(34) Wilhelm, E. Solubilities, Fugacities and All That in Solution Chemistry. *J. Solution Chem.* **2015**, *44*, 1004–1061.

(35) Brunner, G. Properties of Mixtures with Water. *Supercritical Fluid Science and Technology*; American Chemical Society, 2014; Chapter 3, pp 95–225.

(36) Fernández-Prini, R.; Alvarez, J. L.; Harvey, A. H. Henry's Constants and Vapor-Liquid Distribution Constants for Gaseous Solutes in H_2O and D_2O at High Temperatures. *J. Phys. Chem. Ref. Data* **2003**, *32*, 903–916.

(37) Krause, D.; Benson, B. B. The Solubility and Isotopic Fractionation of Gases in Dilute Aqueous Solution. IIa. Solubilities of the Noble Gases. *J. Solution Chem.* **1989**, *18*, 823–873.

(38) Japas, M. L.; Sengers, J. M. H. L. Gas Solubility and Henry's Law near the Solvent's Critical Point. *AIChE J.* **1989**, *35*, 705–713.

(39) Sengers, J. V.; Sengers, J. M. H. L. Thermodynamic Behavior of Fluids near the Critical Point. *Annu. Rev. Phys. Chem.* **1986**, *37*, 189–222.

(40) Lemmon, E. W.; Bell, I. H.; Huber, M. L.; McLinden, M. O. *REFPROP Documentation, Release 10.0*; NIST, 2018; p 135.

(41) Davalos, J.; Anderson, W. R.; Phelps, R. E.; Kidnay, A. J. Liquid-Vapor Equilibria at 250.00K for Systems Containing Methane, Ethane, and Carbon Dioxide. *J. Chem. Eng. Data* **1976**, *21*, 81–84.

(42) Xu, N.; Dong, J.; Wang, Y.; Shi, J. High Pressure Vapor Liquid Equilibria at 293 K for Systems Containing Nitrogen, Methane and Carbon Dioxide. *Fluid Phase Equilib.* **1992**, *81*, 175–186.

(43) Coquelet, C.; Valtz, A.; Dieu, F.; Richon, D.; Arpentinier, P.; Lockwood, F. Isothermal P, x, y Data for the Argon + Carbon Dioxide

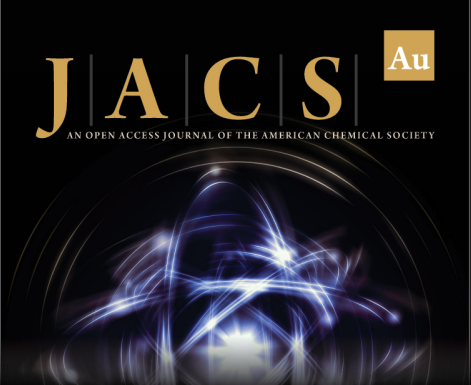
System at Six Temperatures from 233.32 to 299.21 K and Pressures up to 14 MPa. *Fluid Phase Equilib.* **2008**, *273*, 38–43.

(44) Al-Sahhaf, T. A.; Kidnay, A. J.; Sloan, E. D. Liquid + Vapor Equilibria in the $\text{N}_2 + \text{CO}_2 + \text{CH}_4$ System. *Ind. Eng. Chem. Fundam.* **1983**, *22*, 372–380.

(45) Wei, M. S.-W.; Brown, T. S.; Kidnay, A. J.; Sloan, E. D. Vapor + Liquid Equilibria for the Ternary System Methane + Ethane + Carbon Dioxide at 230 K and Its Constituent Binaries at Temperatures from 207 to 270 K. *J. Chem. Eng. Data* **1995**, *40*, 726–731.


(46) Glass, R. W.; Barker, R. E. *A Generalized Computer Model the KALC Process*, 1978. Report ORNL/TM-6242.


(47) Span, R.; Wagner, W. A New Equation of State for Carbon Dioxide Covering the Fluid Region from the Triple Point Temperature to 1100 K at Pressures up to 800 MPa. *J. Phys. Chem. B* **1996**, *25*, 1509–1596.



JACS Au
AN OPEN ACCESS JOURNAL OF THE AMERICAN CHEMICAL SOCIETY

Editor-in-Chief
Prof. Christopher W. Jones
Georgia Institute of Technology, USA

Open for Submissions 

pubs.acs.org/jacsau  ACS Publications
Most Trusted. Most Cited. Most Read.